Inkjet Printed Single-Walled Carbon Nanotube Based Ambipolar and Unipolar Transistors for High-Performance Complementary Logic Circuits

Bucella, Sadir Gabriele; Salazar-Rios, Jorge Mario; Derenskyi, Vladimir; Fritsch, Martin; Scherf, Ullrich; Loi, Maria Antonietta; Caironi, Mario

Published in:
Advanced electronic materials

DOI:
10.1002/aelm.201600094

ADVANCED ELECTRONIC MATERIALS
www.advelectronicmat.de

Inkjet Printed Single-Walled Carbon Nanotube Based Ambipolar and Unipolar Transistors for High-Performance Complementary Logic Circuits

*Sadir Gabriele Bucella, Jorge Mario Salazar-Rios, Vladimir Derenskyi, Martin Fritsch, Ullrich Scherf, Maria Antonietta Loi, and Mario Caironi**

Direct printing technologies, compatible with mass production,[1,2] can enable large-area electronics for wearable, portable, and distributed micro/opto-electronics and sensing applications.[3–8] Different solution-processable semiconductors are being developed and tested in field-effect transistors (FETs), among which conjugated small-molecule and polymer semiconductors are one of the most investigated approaches.[9–14] Alternative carbon based and solution-processable semiconductors, such as single-walled carbon nanotubes (SWCNT),[15] are being also strongly explored because they offer a path towards high performance in terms of charge mobility and electronic bandwidth of printed FETs thanks to their intrinsic electronic properties.[16–18] Printed networks of semiconducting SWCNT[19] can achieve the goal if current challenges in terms of uniform printability and of high purity with controlled chirality of SWCNT formulations are overcome.

The efficient separation of metallic (m-SWNT) and semiconducting (s-SWNT) species in a printable formulation with high loading has commonly represented one of the most difficult hurdles to enable carbon nanotubes based printed electronics with suitable performances, especially for obtaining high on–off ratios and ideal operation of the devices required by logic circuit applications.

Over the past decade, a vast variety of methods have been proposed to sort SWCNTs and obtain high purity printable solutions.[20,21] Among those, non-covalent functionalization through conjugated polymers chains is proving to be a powerful approach for the high-yield sorting of s-SWCNTs and the production of stable dispersions.[22–26] Following this approach, high mobility FETs, with values up to 33 $cm^2 V^{-1} s^{-1}$ and on–off ratios up to 10^8 have been recently demonstrated by adopting coating techniques such casting or blade-coating.[21,24,27,28] Scalable printing techniques enabling the patterning of the semiconductor would also be important in allowing the deposition of controlled volumes in specific areas of circuits thus reducing materials waste, parasitism and enabling complex circuits fabrication. So far direct writing techniques, such as aerosol-jet printing and inkjet printing, have been adopted to pattern non-sorted CNTs[29,30] and low purity s-SWCNTs[31] dispersed in different solvents, obtaining FETs with low on–off ratios and currents hysteresis. Excellent results in terms of mobility were obtained with aerosol jet printing and inkjet printing of s-SWCNTs sorted in water with surfactants by density gradient centrifugation, while typically requiring post-processing on the printed network to improve device performances.[32–36] Only recently, s-SWCNTs sorted in organic solvents by non-covalent functionalization with polymers have been patterned by inkjet printing showing p-type only operation, with saturation mobility of 0.5 $cm^2 V^{-1} s^{-1}$.[37] Owing to the low loading of dispersed nanotubes, 10 printing passes were needed to obtain a working connected network of nanotubes. Here we take advantage of a polymer sorted high quality s-SWCNT ink with concentration of 0.2 g L^{-1} to demonstrate high mobility, inkjet printed FETs which display a high on–off ratio and a suppressed hysteresis, already with a single printing pass, without the need of post-processing. Very interestingly, we show both the possibility to retain balanced ambipolar transport in inkjet printed s-SWCNTs networks processed in ambient atmosphere at low temperature, with mobilities up to 10 $cm^2 V^{-1} s^{-1}$, for holes, and 7 $cm^2 V^{-1} s^{-1}$, for electrons, and to suppress electrons transport, while maintaining high hole mobility up to 15 $cm^2 V^{-1} s^{-1}$, through multi-layer printing thus achieving p-type unipolar devices starting from the same ink. Integration in a complementary-like inverter demonstrates the suitability of polymer sorted s-SWCNTs for the development of high performance printed logic circuits.

To formulate the s-SWCNTs based ink for the inkjet printing process, semiconducting nanotubes were selected from a starting mixture produced by high-pressure carbon monoxide conversion (HiPCO), by adopting poly(3-dodecylthiophene-2,5-diyl) (P3DDT) as wrapping polymer.[38] Inks with up to 0.2 g L^{-1} concentration were found to be the most efficient for printing; higher concentration inks resulted in nozzle clogging.

Dr. S. G. Bucella, Dr. M. Caironi
Center for Nano Science and Technology @PoliMi
Istituto Italiano di Tecnologia
Via Pascoli 70/3, 20133 Milano, Italy
E-mail: mario.caironi@iit.it
Dr. S.G. Bucella
Dipartimento di Fisica
Politecnico di Milano
P.za L. da Vinci 32, 20133 Milano, Italy
J. M. Salazar-Rios, V. Derenskyi, Prof. M. A. Loi
Zernike institute for Advanced Materials
University of Groningen
Nijenborgh 4, Groningen, 9747 AG, The Netherlands
M. Fritsch, Prof. U. Scherf
Macromolecular Chemistry group and Institute for Polymer Technology
Bergische Universität Wuppertal
Gauss-Str. 20, D-42119 Wuppertal, Germany

The copyright line of this paper was amended 1 August 2016 after initial publication.

DOI: 10.1002/aelm.201600094

ADVANCED ELECTRONIC MATERIALS
www.advelectronicmat.de

Materials Views
www.MaterialsViews.com

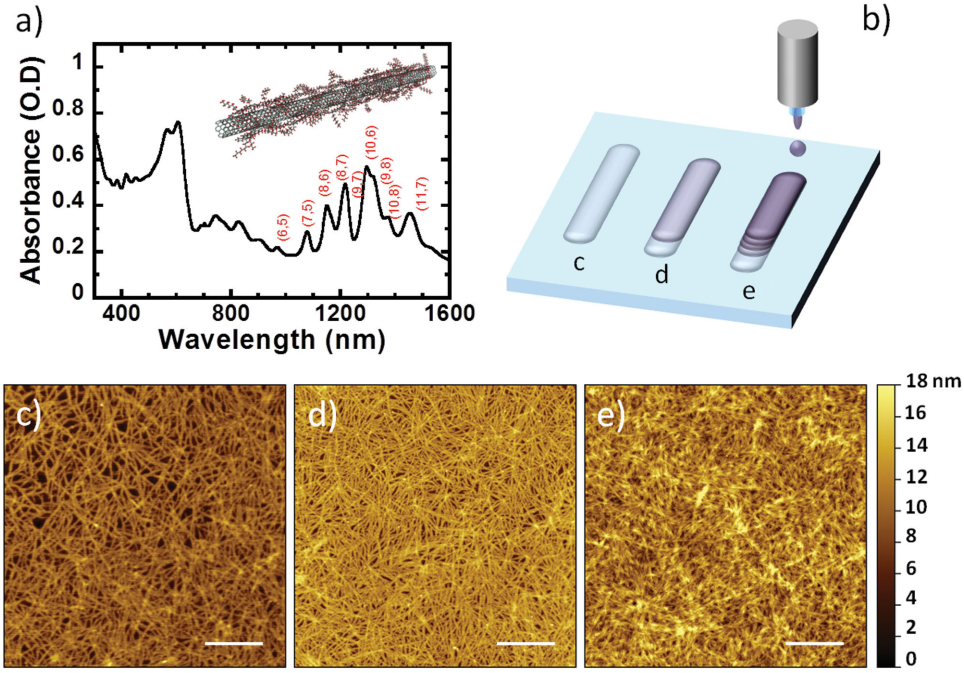

Figure 1. a) Absorption spectrum of HiPCO:P3DDT in ODCB after second centrifugation. The chiralities of the SWNTs present in the sample are determined using an empirical equation.[48,49] In the inset, the structure of SWCNT-P3DDT hybrid is displayed. b) Sketch of the inkjet printing process for the deposition of s-SWCNTs solution. The nozzle diameter adopted has an orifice diameter of 60 μm. The spacing between consecutive drops was set at 100 μm and the printing speed was 50 mm s^{-1}. AFM maps of s-SWCNTs networks obtained by: c) one printing pass, d) two printing passes, and e) six printing passes. Scale bars, 1 μm.

We first obtained a stable dispersion in toluene, according to a previous work[28,39] (absorption spectrum of the solution is reported in Figure S1a in the Supporting Information). However, toluene does not represent an ideal choice for the inkjet printing process, due to its low boiling point. This produces the early evaporation of the formulation at the fluid meniscus at the nozzle orifice, resulting in an unstable jet of ink and loss of patterning resolution (see Section 1 in the Supporting Information). To overcome the problem, the toluene based dispersion was ultracentrifugated to precipitate and separate the s-SWCNTs from the solvent. The resulting solid pellet was then re-dispersed in ortho-dichlorobenzene (oDCB), largely adopted for the printing of organic semiconducting materials, but not so far investigated for deposition of polymer wrapped s-SWCNT dispersion, obtaining a stable dispersion over the entire duration of the fabrication process (more details in Figure S1, Supporting Information). In **Figure 1**a the absorption spectrum of the s-SWCNTs dispersion in oDCB, with which a stable jetting was achieved, is reported.

We deposited the P3DDT wrapped s-SWCNTs solution in oDCB by inkjet printing, in a single or multiple passes, controlled amounts with an orifice nozzle diameter of 60 μm (Figure 1b). The evolution of the films topography with multiple printing passes has been investigated by atomic force microscopy (Figure 1c–e). We observed a uniform and well inter-connected network of nanotubes, with a total coverage of ≈80% already after a single printing pass, highlighting the positive effect of the optimal loading achieved in the solution. An increasing density is observed as a function of the number of printed layers, reaching ≈92% coverage after two printing passes and an almost full coverage of the surface after five passes.

To study the electrical properties of the printed s-SWCNTs networks we adopted a top gate, bottom contacts FET architecture (**Figure 2**a), where a varying number of s-SWCNTs layers were inkjet printed on pre-patterned gold source and drain electrodes. All the printing processes have been performed in ambient air, at room temperature. Typical transfer (left) and output (right) characteristic curves of the printed FETs are reported in Figure 2b–d. Interestingly, the single (b) and two passes (c) printed layers devices, besides being characterized by a very good level of surface coverage, exhibit clean and balanced ambipolar characteristics, something not achieved in previous works,[28,37] where holes transports dominated. Higher channel (I_{DS}) currents are measured as a result of the higher network coverage, due to the second printing pass, for both accumulation regimes. The on–off ratios calculated at V_{DS} = ±5V are between 10^6 and 10^7 for both the electron and hole accumulations. By starting from the third pass (Figure S2, Supporting Information), a different trend can be observed, with a substantial saturation of the holes current and a neat decrease of the electron current. As a result of this trend, with more than five printed layers, as the case of the six printed layer reported in Figure 2d, the device shows a drastic unbalanced ambipolar behavior, with currents comparable to the two passes device in holes accumulation regime, while an order of magnitude lower currents in electron accumulation regime. The device obtained by six printing passes substantially embodies a unipolar device.

While the on–off ratio of the electron accumulation is evidently lowered, due to the lowering of the on currents, that

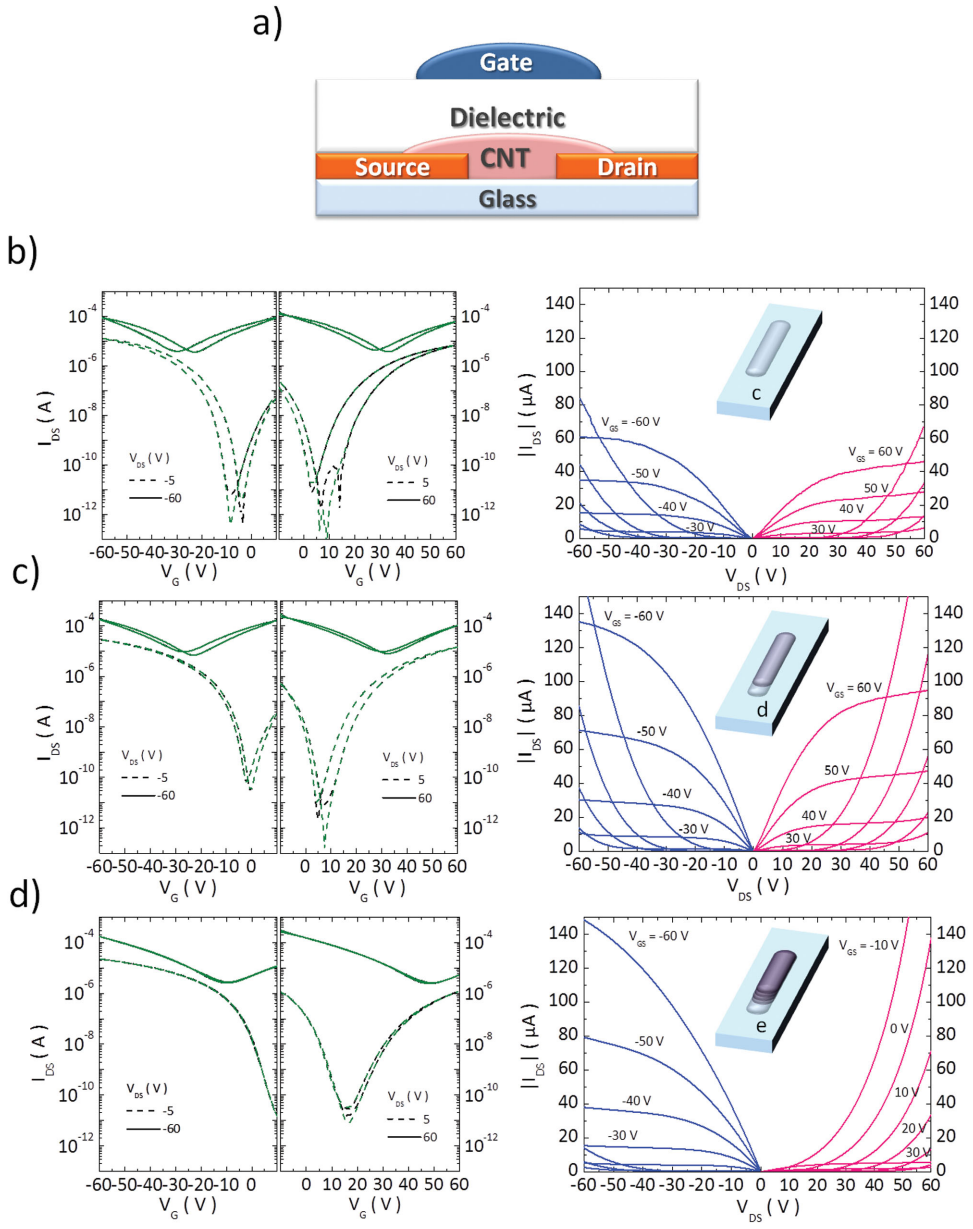

Figure 2. a) Sketch of the top gate-bottom contacts geometry adopted for the fabrication of SWCNTs based FET (channel width W = 200 μm and channel length L = 40 μm). b–d) Transfer characteristic (left) and output (right) measurements of devices made with: a) one printed pass, b) two printed passes, and c) more than five printed passes of SWCNTs.

of the hole accumulation is still close to 10^6 with more than three passes. While in previous works, in order to maintain on–off ratios of about 10^4, networks with limited coverage were adopted,[32,33] likely to reduce the negative effect of residual metallic nanotubes, the high purity of the ink adopted in this work allows the almost full coverage of the surface without negatively affecting the on–off ratio.

We notice a very limited hysteresis in the hole currents, slightly more pronounced in the electron currents, only with one and two printing passes, while it basically disappears with more printing passes. We tentatively assign the small hysteretic behavior of devices with one and two printing passes to the effect of the interaction with water and/or –OH groups present on the glass surface,[40] which forms a less ideal interface than the one between s-SWCNT and the polymer dielectric. Such an effect is likely screened with thicker networks.

From the characteristic curves of the devices we have extracted the threshold voltages (V_{th}) and the field effect mobilities as a function of the number of printing passes, both in the linear ($|V_{GS}|$ = 60 V and $|V_{DS}|$ = 5 V, **Figure 3**, empty symbols) and the saturation regime ($|V_{GS}|$ = 60 V and $|V_{DS}|$ = 60 V, Figure 3, filled symbols), for both the holes (blue) and electrons (red). While the holes mobility increases with the number of passes, saturating after three, the electrons mobility shows a peak with two printing passes and then monotonically decreases. For two printing passes, balanced holes ($\mu_{lin\text{-}hole}$)

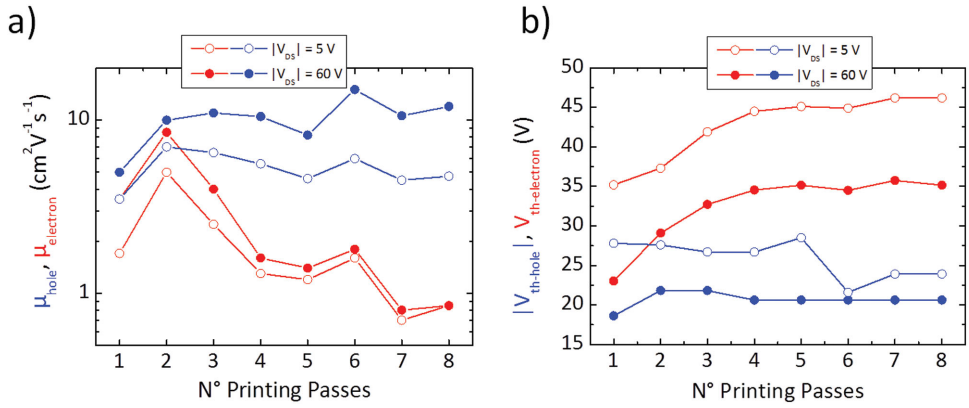

Figure 3. a) Mobility plot extracted from devices made by increasing the number of printed passes (channel width $W = 200$ μm and channel length $L = 40$ μm). The holes mobility (blue lines) and electrons mobility (red lines) in linear regime (empty symbols) and saturation regime (filled symbols) are reported. b) Threshold voltages of the same devices.

and electrons ($\mu_{\text{lin-electron}}$) linear mobility of 7 and 5 cm^2 V^{-1} s^{-1}, respectively, were extracted using the gradual-channel approximation and the parallel plates capacitor model; for the same printing condition, saturation mobility for holes ($\mu_{\text{sat-hole}}$) and electrons ($\mu_{\text{sat-electron}}$) are 10 and 7 cm^2 V^{-1} s^{-1}, respectively. With multiple printing passes a maximum $\mu_{\text{sat-hole}}$ of 15 cm^2 V^{-1} s^{-1}, among the highest so far reported for an inkjet printed s-SWCNTs based device, was obtained. The trend of V_{th}, which is approximately constant for holes accumulation and increases for the electrons, is in agreement with the mobility trends, confirming a lowering in electron accumulation and transport efficiency. We have here reported the best data obtained. In Figures S2.3 and S2.4 in the Supporting Information, we have included data obtained with three different formulation batches and 48 devices in total (6 per number of printed passes). Electron mobilities in the range or higher than 1 cm^2 V^{-1} s^{-1} were observed for all batches with up to three printed passes; they do always show a decreasing trend with printed passes. Concerning holes transport, mobility values well above 1 cm^2 V^{-1} s^{-1} were measured independently of the batch adopted and of the printed passes.

The effect observed with multiple passes can be rationalized by considering two different regimes: the first with one and two printing passes, and the second for three passes or more. In the first regime, we observe an increase of the currents as a result of a denser network obtained, in agreement with AFM images in Figure 1c,d. We suggest that the increase in carrier mobility is related to a geometrical factor as well as to the higher number of connections between electrodes and nanotubes. This increase in connectivity allows the formation of more efficient percolation paths for the charges. Starting from the third printing pass, the s-SWCNTs start to stratify with negligible further increase in the coverage. This explains the saturation in holes currents and corresponding mobility, suggesting at the same time that the top s-SWCNTs form an as good transporting network as the bottom ones. Concerning the electron current the same consideration for the first regime is valid but a decreasing trend is present in the second regime. To explain this effect we have investigated the correlation between the number of printed layers, and the contact and channel resistances, for both holes and electrons, by using the differential method (DM)[41,42] and G-function method[43] (for details please see Supporting Information, Section 3: Contact Resistance Extraction). While an increasing trend in channel resistance for the electron is clearly visible, the contact resistance values are approximately constant within increasing printing passes. Differently, constant values of both channel and contact resistance are extracted for the holes by increasing the number of printing passes. We can speculate that with additional layers, after the injection from the metal into semiconductor, the electron has to overcome barriers due to trap states introduced by the increasing amount of the residual or segregated sorting polymer P3DDT, which is a good hole/poor electron transporting material[38] (see the Supporting information, Section 4: Effect of the polymer).

The demonstrated ambipolarity and the fine control of the charge transport through the number of printing passes gave us the possibility to fabricate complementary logic using the same ink. As a proof of concept we fabricated the simplest complementary logic circuit possible, an inverter, the scheme of which is reported in **Figure 4**a. To obtain devices with balanced on-state currents and similar V_{th}, important parameters for the fabrication of an ideal inverter, we adopted a three printing passes transistor for the p-type device and a two passes device was selected for the n-type. In Figure 4b, the typical input–output voltage transfer characteristic of the inverter (black) and the gain (red) are reported, demonstrating a clear inverting behavior. For V_{DD} up to 30 V, the transition is almost rail-to-rail, i.e., the output switches from V_{DD} to 0 V. For higher V_{DD} in both logic states the rail is not reached because of the residual parasitic n-type currents in the p-type device and the balanced ambipolarity of the n-type device. Despite this non-ideality, the threshold voltage is close to the ideality, i.e., $V_{\text{DD}}/2$, as an effect of balanced hole and electron currents and threshold voltages. Noise margins, extracted according to the maximum square method,[44] are close to 20 at $V_{\text{DD}} = 60$ V, as well as the gain, which is higher than 10 already at $V_{\text{DD}} = 20$ V and reaches a maximum of 18.6 at $V_{\text{DD}} = 60$ V. The fabricated inverter therefore demonstrates a building block compatible with the realization of high-performance and robust logic circuits based on printed s-SWCNTs.

In summary, a direct writing inkjet printing technique has been adopted for the fine deposition of s-SWCNTs with

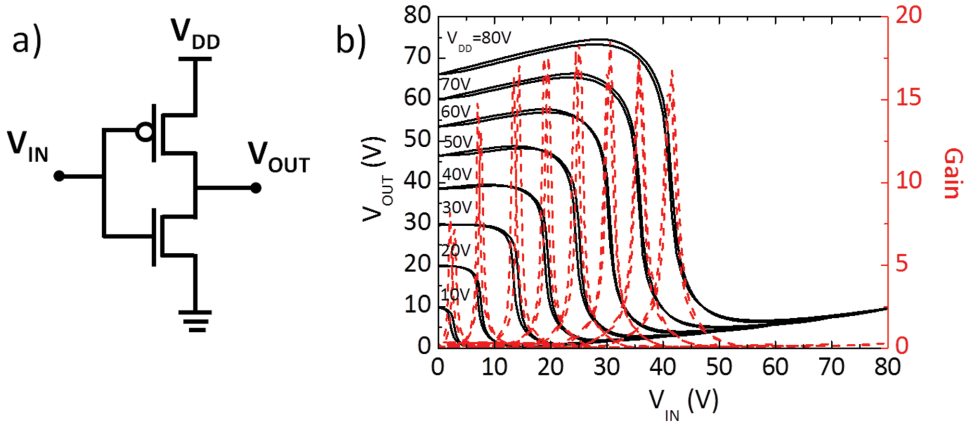

Figure 4. a) Circuital scheme of an inverter. b) Measured inverter transfer characteristic (black) and gain (red) of ambipolar printed SWCNTs devices.

excellent transport properties. We employed a high-yield sorting method based on non-covalent functionalization through P3DDT chains to select only semiconducting chirality. Through an enrichment process, a stable formulation in oDCB with high loading (up to 0.2 mg mL^{-1}) has been obtained resulting in a dense network of nanotubes already after a single printing pass. By varying the printing passes, balanced ambipolar FETs, with saturation mobilities of 10 and 7 cm^2 V^{-1} s^{-1}, for holes and electrons respectively, as well as unipolar p-type FETs, with a maximum saturation mobility of 15 cm^2 V^{-1} s^{-1}, have been realized, showing hysteretic free behavior and on–off ratio in linear regime up to 10^7. While further studies are required to assess the detailed role of the wrapping and/or residual polymer in the electronic properties of the printed layers, we have suggested a method to reliably formulate fairly stable and printable dispersions of s-SWCNTs with controllable ambipolar electrical properties. This allowed the fabrication of a complementary-like inverter displaying a clear inverting behavior, a gain of 18.6 and a noise margin up to 20. s-SWCNT inkjet printed transistors here demonstrated are very promising for high performance large-area and flexible electronics, enabling improved computation complexity and high frequency switching speed, with an expected transition frequency[45] well above 10 MHz already for simple device architectures compatible with cost-effective, scalable manufacturing processes.[46]

Experimental Section

SWCNTs Based Ink Preparation: Poly(3-dodecylthiophene-2,5-diyl) was synthesized via GRIM method.[47] The molecular weight (M_n = 26.800 g mol^{-1}, M_w = 29.000 g mol^{-1}) was determined by gel permeation chromatography (GPC). HiPCO SWNTs were purchased from Unidym, Inc. and were used as received.

The polymer was solubilized in toluene using a high power ultrasonicator (Misonix 3000) with cup horn bath (output power 69 W). Subsequently, SWNTs were added to form the HiPco:polymer dispersions with weight ratio 1:2. The solution was then sonicated for 2 h at 69 W and 16 °C. After ultrasonication, the dispersion was centrifuged at 40 000 rpm (196 000 *g*) for 1 h in an ultracentrifuge (Beckman Coulter Optima XE-90; rotor: SW55Ti) to remove all the remaining bundles and heavy-weight impurities. After the centrifugation, the highest density components precipitate at the bottom of the centrifugation tube, while the low density components, including individualized s-SWNTs wrapped by the polymer and free polymer chains, stay in the upper part as supernatant. An extra step of ultracentrifugation was implemented to decrease the amount of free polymer in solution (enrichment).[27] For this purpose, the supernatant obtained after the first ultracentrifugation was centrifuged for 5 h, 55 000 rpm (367 000 *g*), the individualized s-SWNTs were now precipitated to form a pellet and the free polymer was kept in the supernatant. Finally, the pellet was redispersed by mild sonication in oDCB.

Optical measurements were performed using a UV–vis–NIR spectrophotometer (Shimadzu UV-3600) to check the concentration of the carbon nanotubes selected by the polymers, as well as the amount of the polymer in the solution.

Samples and Devices Fabrication: Low alkali 1737F Corning glasses were used as substrates for films and devices realized in this work. A standard cleaning in ultrasonic bath of Milli-Q water, acetone and isopropyl alcohol respectively and a following exposition to O_2-plasma at 100 W were employed. Top-Gate, Bottom Staggered-contacts geometry was chosen for the realization of FETs. Bottom electrodes were patterned by a lift-off photolithographic process and deposited by evaporation of a 1.5 nm thick Cr adhesion layer and 15 nm thick Au film. Patterned substrates were cleaned by ultrasonic bath in isopropyl alcohol for 2–3 min and exposed to O_2-plasma at 100 W for 10 min before the printing of nanotubes. A custom inkjet printing system, Jetlab 4xl-A, provided with a nozzle with orifice diameter of 60 µm, was adopted for the deposition of SWCNTs based ink as semiconducting layer. After the printing the devices were annealed on a hotplate for 14 h at 120 °C in Nitrogen atmosphere. PMMA (Sigma-Aldrich) with M_w = 120 kg mol^{-1} was spun from *n*-butyl acetate (80 g L^{-1}). Dielectric layers with thickness between 500–600 nm were obtained. After the dielectric deposition, the devices were annealed under nitrogen, on a hot-plate, at 80 °C for 30 min. The device was completed by inkjet printing a commercial PEDOT:PSS formulation (Heraeus Clevios P Jet 700) serving as a gate electrode. At this scope, a Fujifilm Dimatix Materials Printer DMP-2831 (10 pl drops volume cartridge) was used.

Film morphology Characterization: The surface topography of the films was measured with an Agilent 5500 Atomic Force Microscope operated in the Acoustic Mode. Optical measurements were performed using a UV–vis–NIR spectrophotometer (Shimadzu UV-3600) to check the concentration of the carbon nanotubes selected by the polymers, as well as the amount of the polymer in the solution.

Electrical Characterization: The electrical characteristics of transistors were measured in a nitrogen glovebox on a Wentworth Laboratories probe station with a semiconductor device analyzer (Agilent B1500A). The linear and saturation mobility values were calculated using the gradual-channel approximation, according to the parallel plate model. The mobility data reported do not take into account contact effects, i.e., the data correspond to an effective mobility.

Supporting Information

Supporting Information is available from the Wiley Online Library or from the author.

Acknowledgements

The authors acknowledge Francesca Scuratti for the support in the fabrication processes. This work has been financially supported by the European Research Council (ERC) under the European Union's Horizon 2020 research and innovation program 'HEROIC', grant agreement 638059. The collaborative research program between the University of Groningen and Wuppertal University was made possible with financial support by Stichting voor de Technische Wetenschappen (STW, Utrecht, the Netherlands) and the Deutsche Forschungsgemeinschaft (DFG, Bonn, Germany).

Received: March 3, 2016
Revised: April 4, 2016
Published online: April 26, 2016

[1] K.-J. Baeg, M. Caironi, Y.-Y. Noh, *Adv. Mater.* **2013**, *25*, 4210.
[2] Y. Aleeva, B. Pignataro, *J. Mater. Chem. C* **2014**, *2*, 6436.
[3] T. Sekitani, M. Takamiya, Y. Noguchi, S. Nakano, Y. Kato, T. Sakurai, T. Someya, *Nat. Mater.* **2007**, *6*, 413.
[4] A. C. Arias, J. D. MacKenzie, I. McCulloch, J. Rivnay, A. Salleo, *Chem. Rev.* **2010**, *110*, 3.
[5] G. Gelinck, P. Heremans, K. Nomoto, T. D. Anthopoulos, *Adv. Mater.* **2010**, *22*, 3778.
[6] T. Someya, A. Dodabalapur, J. Huang, K. C. See, H. E. Katz, *Adv. Mater.* **2010**, *22*, 3799.
[7] M. Singh, H. M. Haverinen, P. Dhagat, G. E. Jabbour, *Adv. Mater.* **2010**, *22*, 673.
[8] G. Pace, A. Grimoldi, D. Natali, M. Sampietro, J. E. Coughlin, G. C. Bazan, M. Caironi, *Adv. Mater.* **2014**, *26*, 6773.
[9] H. Usta, A. Facchetti, T. J. Marks, *Acc. Chem. Res.* **2011**, *44*, 501.
[10] A. Facchetti, *Chem. Mater.* **2011**, *23*, 733.
[11] C. Ruiz, E. M. García-Frutos, G. Hennrich, B. Gómez-Lor, *J. Phys. Chem. Lett.* **2012**, *3*, 1428.
[12] S. Kola, J. Sinha, H. E. Katz, *J. Polym. Sci. Part B Polym. Phys.* **2012**, *50*, 1090.
[13] J. Mei, Y. Diao, A. L. Appleton, L. Fang, Z. Bao, *J. Am. Chem. Soc.* **2013**, *135*, 6724.
[14] D. Khim, K.-J. Baeg, M. Caironi, C. Liu, Y. Xu, D.-Y. Kim, Y.-Y. Noh, *Adv. Funct. Mater.* **2014**, *24*, 6252.
[15] J. W. G. Wilder, L. C. Venema, A. G. Rinzler, R. E. Smalley, C. Dekker, *Nature* **1998**, *391*, 59.
[16] C. T. White, T. N. Todorov, *Nature* **1998**, *393*, 240.
[17] T. Dürkop, S. a. Getty, E. Cobas, M. S. Fuhrer, *Nano Lett.* **2004**, *4*, 35.
[18] Y. M. Lin, J. Appenzeller, J. Knoch, P. Avouris, *IEEE Trans. Nanotechnol.* **2005**, *4*, 481.
[19] J. Zaumseil, *Semicond. Sci. Technol.* **2015**, *30*, 074001.
[20] M. C. Hersam, *Nat. Nanotechnol.* **2008**, *3*, 387.
[21] S. K. Samanta, M. Fritsch, U. Scherf, W. Gomulya, S. Z. Bisri, M. A. Loi, *Acc. Chem. Res.* **2014**, *47*, 2446.
[22] H. W. Lee, Y. Yoon, S. Park, J. H. Oh, S. Hong, L. S. Liyanage, H. Wang, S. Morishita, N. Patil, Y. J. Park, J. J. Park, A. Spakowitz, G. Galli, F. Gygi, P. H.-S. Wong, J. B.-H. Tok, J. M. Kim, Z. Bao, *Nat. Commun.* **2011**, *2*, 541.
[23] J. Gao, M. A. Loi, E. J. F. De Carvalho, M. C. Dos Santos, *ACS Nano* **2011**, *5*, 3993.
[24] W. Gomulya, G. D. Costanzo, E. J. F. de Carvalho, S. Z. Bisri, V. Derenskyi, M. Fritsch, N. Fröhlich, S. Allard, P. Gordiichuk, A. Herrmann, S. J. Marrink, M. C. dos Santos, U. Scherf, M. A. Loi, *Adv. Mater.* **2013**, *25*, 2948.
[25] H. Wang, G. I. Koleilat, P. Liu, G. Jiménez-Osés, Y. C. Lai, M. Vosgueritchian, Y. Fang, S. Park, K. N. Houk, Z. Bao, *ACS Nano* **2014**, *8*, 2609.
[26] S. P. Schiessl, N. Fröhlich, M. Held, F. Gannott, M. Schweiger, M. Forster, U. Scherf, J. Zaumseil, S. P. Schießl, N. Fro, M. Held, F. Gannott, M. Schweiger, M. Forster, U. Scherf, J. Zaumseil, *ACS Appl. Mater. Interfaces* **2015**, *7*, 682.
[27] S. Z. Bisri, J. Gao, V. Derenskyi, W. Gomulya, I. Iezhokin, P. Gordiichuk, A. Herrmann, M. A. Loi, *Adv. Mater.* **2012**, *24*, 6147.
[28] V. Derenskyi, W. Gomulya, J. M. S. Rios, M. Fritsch, N. Fröhlich, S. Jung, S. Allard, S. Z. Bisri, P. Gordiichuk, A. Herrmann, U. Scherf, M. A. Loi, *Adv. Mater.* **2014**, *26*, 5969.
[29] P. Beecher, P. Servati, A. Rozhin, A. Colli, V. Scardaci, S. Pisana, T. Hasan, A. J. Flewitt, J. Robertson, G. W. Hsieh, F. M. Li, A. Nathan, A. C. Ferrari, W. I. Milne, *J. Appl. Phys.* **2007**, *102*, 043710.
[30] H. Okimoto, T. Takenobu, K. Yanagi, Y. Miyata, H. Shimotani, H. Kataura, Y. Iwasa, *Adv. Mater.* **2010**, *22*, 3981.
[31] J. Zhao, Y. Gao, W. Gu, C. Wang, J. Lin, Z. Chen, Z. Cui, *J. Mater. Chem.* **2012**, *22*, 20747.
[32] M. Ha, Y. Xia, A. a. Green, W. Zhang, M. J. Renn, C. H. Kim, M. C. Hersam, C. D. Frisbie, *ACS Nano* **2010**, *4*, 4388.
[33] M. Ha, J. W. T. Seo, P. L. Prabhumirashi, W. Zhang, M. L. Geier, M. J. Renn, C. H. Kim, M. C. Hersam, C. D. Frisbie, *Nano Lett.* **2013**, *13*, 954.
[34] F. Sajed, C. Rutherglen, *Appl. Phys. Lett.* **2013**, *103*, 8.
[35] B. Kim, S. Jang, P. L. Prabhumirashi, M. L. Geier, M. C. Hersam, B. Kim, S. Jang, P. L. Prabhumirashi, M. L. Geier, *Appl. Phys. Lett.* **2013**, *082119*, 2.
[36] B. Kim, S. Jang, M. L. Geier, P. L. Prabhumirashi, M. C. Hersam, A. Dodabalapur, *Nano Lett.* **2014**, *14*, 3683.
[37] H. Wang, B. Hsieh, G. Jiménez-Osés, P. Liu, C. J. Tassone, Y. Diao, T. Lei, K. N. Houk, Z. Bao, *Small* **2015**, *11*, 126.
[38] S. Scheinert, G. Paasch, M. Schrödner, H.-K. Roth, S. Sensfuß, T. Doll, *J. Appl. Phys.* **2002**, *92*, 330.
[39] W. Gomulya, J. M. Salazar Rios, V. Derenskyi, S. Z. Bisri, S. Jung, M. Fritsch, S. Allard, U. Scherf, M. C. dos Santos, M. A. Loi, *Carbon N. Y.* **2015**, *84*, 66.
[40] W. Kim, a. Javey, O. Vermesh, O. Wang, Y. M. Li, H. J. Dai, *Nano Lett.* **2003**, *3*, 193.
[41] D. Natali, L. Fumagalli, M. Sampietro, *J. Appl. Phys.* **2007**, *101*.
[42] D. Natali, M. Caironi, *Adv. Mater.* **2012**, *24*, 1357.
[43] C. Liu, T. Minari, Y. Xu, B. Yang, H.-X. Chen, Q. Ke, X. Liu, H. C. Hsiao, C. Y. Lee, Y.-Y. Noh, *Org. Electron.* **2015**, *27*, 253.
[44] J. R. Hauser, *IEEE Trans. Educ.* **1993**, *36*, 363.
[45] M. Caironi, Y.-Y. Noh, H. Sirringhaus, *Semicond. Sci. Technol.* **2011**, *26*.
[46] S. G. Bucella, A. Luzio, E. Gann, L. Thomsen, C. R. McNeill, G. Pace, A. Perinot, Z. Chen, A. Facchetti, M. Caironi, *Nat. Commun.* **2015**, *6*, 8394.
[47] R. S. Loewe, S. M. Khersonsky, R. D. McCullough, *Adv. Mater.* **1999**, *11*, 250.
[48] H. Kataura, Y. Kumazawa, Y. Maniwa, I. Umezu, S. Suzuki, Y. Ohtsuka, Y. Achiba, *Synth. Met.* **1999**, *103*, 2555.
[49] J. H. Choi, M. S. Strano, *Appl. Phys. Lett.* **2007**, *90*, 223114.